International Journal of Solids and Structures 50 (2013) 2527–2541

Contents lists available at SciVerse ScienceDirect

International Journal of Solids and Structures

journal homepage: www.elsevier.com/locate/ijsolstr

# Computational analysis of multi-stepped beams and beams with linearly-varying heights implementing closed-form finite element formulation for multi-cracked beam elements

Matjaž Skrinar *

*University of Maribor, Faculty of Civil Engineering, Smetanova 17, SI 2000 Maribor, Slovenia*

ARTICLE INFO

*Article history:*
Received 5 October 2012
Received in revised form 12 March 2013
Available online 22 April 2013

*Keywords:*
Stepped beams with transverse cracks
Transversely cracked beams with linearly varying height
Simplified computational model
Principle of virtual work
Finite element method
Stiffness matrix
Load vector
Transverse displacements

ABSTRACT

The model where the cracks are represented by means of internal hinges endowed with rotational springs has been shown to enable simple and effective representation of transversely-cracked slender Euler–Bernoulli beams subjected to small deflections. It, namely, provides reliable results when compared to detailed 2D and 3D models even if the basic linear moment–rotation constitutive law is adopted.

This paper extends the utilisation of this model as it presents the derivation of a closed-form stiffness matrix and a load vector for slender multi-stepped beams and beams with linearly-varying heights. The principle of virtual work allows for the simple inclusion of an arbitrary number of transverse cracks. The derived at matrix and vector define an 'exact' finite element for the utilised simplified computational model. The presented element can be implemented for analysing multi-cracked beams by using just one finite element per structural beam member. The presented expressions for a stepped-beam are not exclusively limited to this kind of height variation, as by proper discretisation an arbitrary variation of a cross-section's height can be adequately modelled.

The accurate displacement functions presented for both types of considered beams complete the derivations. All the presented expressions can be easily utilised for achieving computationally-efficient and truthful analyses.



## 1. Introduction

Numerous engineering structures are subjected to degenerative effects during their utilisation. The progressions of cracks can severely decrease the stiffness of an element and further lead to the failure of the complete structure. In view of this, it is an important task of engineers to detect these cracks as soon as possible. However, the efficiency of structural health monitoring depends not only on the data measured but also on the qualities and versatilities of computational models regarding mechanical behaviour modelling. Undoubtedly, suitable 2D or 3D meshes of finite elements yield a thorough discretisation of the structure, as well as of the crack and its surroundings. Although this approach is excellent when evaluating a structure's response to a cracked situation (with all the crack's details known in advance), it becomes quite awkward for inverse problems where the potential crack's details (presence, location, intensity) are unknown. Consequently, simplified models are more efficient in such situations.

The model that has been the subject of numerous research in the past, is the model provided by Okamura et al. (1969). In this model each crack is replaced by a massless rotational linear spring of suitable stiffness and the linear moment-rotation constitutive law is adopted. Each spring connects those neighbouring non-cracked parts of the beam that are modelled as elastic elements.

Okamura et al. introduced the earliest definition for rotational linear spring stiffness for a rectangular cross-section. In addition, some other researchers (Dimarogonas and Papadopulus, 1983; Rajab and Al-Sabeeh, 1991; Ostachowicz and Krawczuk, 1990; Krawczuk and Ostachowicz, 1993; Sundermayer and Weaver, 1993; Hasan, 1995; Skrinar and Pliberšek, 2004) have presented their definitions.

This model was successfully implemented for dynamic analyses. For a singly-cracked beam Fernández-Sáez and Navarro (2002) presented closed-form expressions for the approximated values of fundamental frequencies, whilst for a beam with multiple cracks several solutions exist for natural frequency calculations: a technique that reduces the order of the determinantal equation (Shifrin and Ruotolo, 1999); a transfer matrix-based method leading to the determinant calculation of a $4 * 4$ matrix (Khiem and Lien, 2001); a fundamental solutions and recurrences formulae-based approach for determining the mode-shapes of non-uniform beams and concentrated masses (Li, 2002). The dynamic response of a cracked cantilever beam subjected to a concentrated moving

* Tel.: +386 2 22 94 358; fax: +386 2 25 24 179.
*E-mail addresses:* matjaz.skrinar@gmail.com, matjaz.skrinar@um.si

0020-7683/$ - see front matter © 2013 Elsevier Ltd. All rights reserved.
http://dx.doi.org/10.1016/j.ijsolstr.2013.04.005

load was studied by Lin and Chang (2006). Dado and Abuzeid (2003) considered the coupling between the bending and axial modes of vibration by implementing axial spring in the crack model.

A general solution for the modal displacement of an Euler–Bernoulli beam with an arbitrary type of discontinuity (with cracks treated as slopes' discontinuities) at an arbitrary number of locations, was presented by Wang and Qiao (2007), where Heaviside's function was used to express the modal displacement of the whole beam by a single function. Exact closed-form expressions for the vibration modes of the Euler–Bernoulli beam, in the presence of multiple concentrated cracks modelled by means of Dirac's deltas, were presented by Caddemi and Caliò (2009). The proposed expressions were explicitly provided as functions of four integration constants only, to be determined by the standard boundary conditions.

Okamura's simplified computational model has also already been implemented regarding experimental inverse identification of a crack: Rizos et al. (1990) measured displacements at two selected points, Boltežar et al. (1998) and Vestroni and Capecchi (2000) implemented eigenfrequencies, Bamnios et al. (2002) used mechanical impedance measurements, and Xiang et al. (2006) discussed a methodology based on B-spline wavelet on the interval element. Further, the utilisation of neural networks to assess the damage in structure from changes in static parameter was discussed by Maity and Saha (2004).

However, since governing differential equations of bending displacement can only be solved analytically for moderate structures, the research interest has further oriented towards a finite element solution for the computation of transverse displacements. The numerical procedure for the computation of a beam element with a single transverse crack was first introduced by Gounaris and Dimarogonas (1988). Skrinar presented, in symbolic forms, the stiffness (Skrinar and Umek, 1996) and geometrical stiffness (Skrinar, 2007) matrices of a beam finite element with an arbitrarily located single transverse crack. An exact solution for the uniform Euler–Bernoulli column in the presence of multiple concentrated cracks, as modelled by means of Dirac's deltas, where the exact explicit expressions of the stability mode shapes as functions of four integration constants only, was obtained by Caddemi and Caliò (2008). Krawczuk et al. (2000) discussed the influence of the plastic zone ahead of the crack tip on the flexibility of the element, thus presenting in closed forms the inertia and stiffness matrices of the element with a mid-span crack. A finite element scheme for computing the eigensystem for a cracked beam for different degrees of closure was developed by Kisa and Brandon (2000).

Several different approaches were applied to obtain closed-form solutions for the static transverse displacements and stiffness matrix of a beam's finite element having an arbitrary number of transverse cracks: implementation of the Dirac delta function either in regard to the rigidity (Biondi and Caddemi, 2007), or flexibility (Palmeri and Cicirello, 2011); sequential solutions of coupled differential equations (Skrinar, 2009); and the principle of virtual work (Skrinar and Pliberšek, 2012). All these solutions, although derived by different mathematical methods, originate from the genuine governing differential equation for the transverse displacements of cracked Euler–Bernoulli beam.

This paper extends the utilisation principle of virtual work in order to obtain a stiffness matrix and a load vector for a uniform load over the whole element and displacements' functions for stepped-beams and beams with linearly-varying heights. Simple and straightforward derivation steps allow for expressions to be given as closed-form solutions.

These explicitly-written expressions not only facilitate the computation but also allow for better examination of the cracks' influences during the static analysis.

## 2. A multi-cracked multi-stepped beam finite element's mathematical model formulation

The discussed multi-stepped-beam finite element considers slender elastic homogeneous Euler–Bernoulli beams subjected to small deflections. The element of total length $L$ is assumed to have a uniform modulus of elasticity $E$ and width $b$. It consists of a sequence of $N_s$ consecutive elastic geometric sections, as shown in Fig. 1. These sections are numbered from the left-end and each section of the element is characterised by a different uniform thickness $h_j$ ($j = 1,2,\ldots,N_s$). The location of the interface between the section $j$ and adjacent section $j+1$ to the right is denoted as $\bar{L}_j$ (with $\bar{L}_o = 0$ and $\bar{L}_{N_s} = L$).

Each section can be either non-cracked or cracked with an arbitrary number of transverse cracks. The cracks are described by a massless rotational springs. Due to the localised effects of the cracks, the adjacent non-cracked parts bordering each crack are modelled as simple elastic sections connected by the rotational spring.

Each crack is assumed to be open with a uniform depth $d_i$. The spring constant $K_i$ is a function of the corresponding non-cracked cross-section's height $h_j$, the relative depth of the crack $\delta_i = d_i/h_j$, Poisson's ratio , and the flexural rigidity $EI_j$ of the neigbouring cracked cross-section $j$. The finite element has altogether $N_c$ cracks at locations (distances) $L_i$ from the left node ($i = 1,2,\ldots,N_c$).

The finite element has four degrees of freedom altogether: transverse displacement $Y_1$ and rotation $\Phi_1$ at the left-end (node 1), as well as transverse displacement $Y_2$ and rotation $\Phi_2$ at the right-end (node 2). Upward displacement and anticlockwise rotations are taken as positive.

## 3. Derivation of stiffness matrix

The four columns of stiffness matrix are obtained from two separate derivations. Since the finite element has four degrees of freedom altogether, this consequently means that in order to obtain a statically determinate structure, two degrees of freedom must be simultaneously removed. In order to complete this, all the required stiffness matrix coefficients are obtained from two cantilever substructures: clamped at both the right and left-ends, respectively.

### 3.1. Cantilever clamped at the right-end

The derivation of the first two columns of stiffness matrix considers a cantilever clamped at the right-end. The structure is subjected to a vertical upward force $F_{n_1}$ and an anticlockwise bending moment $M_{n_1}$ at the free end. Since this is a statically deter-

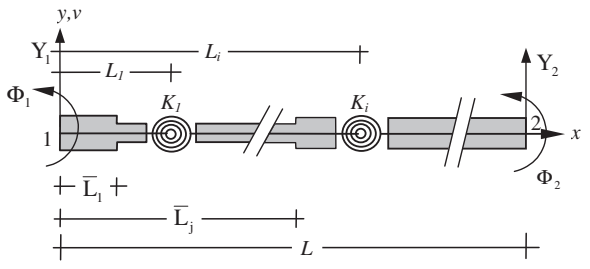


**Fig. 1.** Stepped beam finite element with cracks, nodes and degrees of freedom.

minate structure, the distribution of bending moments due to the applied loads can be obtained from basic equilibriums.

Transverse displacement $Y_1$ and rotation $\Phi_1$ at the left-end due to the acting loads are obtained by implementing the principle of virtual work. Therefore, a virtual vertical upward force $\delta x_1 = 1$ and virtual anticlockwise bending moment $\delta x_2 = 1$ are individually applied at the considered point. The required nodal transverse displacement $Y_1$ is afterwards obtained by integrating the diagrams of bending moments for the structure subjected to the simultaneously applied force $F_{n_1}$ and bending moment $M_{n_1}$, with the diagrams for the structure subjected to the virtual force $\delta x_1$. Consequently, the total displacement is a sum of displacements from both loads:

$$Y_1 = Y_1(F_{n_1} + M_{n_1}) = Y_1(F_{n_1}) + Y_1(M_{n_1}) \tag{1}$$

Similarly, the nodal rotation $\Phi_1$ is obtained by integrating the diagrams for the structure subjected to the applied loads, with the moments' diagram due to the applied virtual bending moment $\delta x_2 = 1$. The rotation also consists of contributions from both loads:

$$\Phi_1 = \Phi_1(F_{n_1} + M_{n_1}) = \Phi_1(F_{n_1}) + \Phi_1(M_{n_1}) \tag{2}$$

*3.1.1. Nodal transverse displacement and nodal rotation for a stepped-beam*

The cantilever utilised for the stepped-beam's stiffness matrix derivation is presented in Fig. 2. For this structure the total transverse nodal displacement $Y_{n_1}$ is expressed as:

$$Y_1 = F_{n_1} \cdot \left( \sum_{i=1}^{N_s} \frac{\overline{L}_i^3 - \overline{L}_{i-1}^3}{3 \cdot EI_i} + \sum_{i=1}^{N_c} \frac{L_i^2}{K_i} \right) - M_{n_1} \cdot \left( \sum_{i=1}^{N_s} \frac{\overline{L}_i^2 - \overline{L}_{i-1}^2}{2 \cdot EI_i} + \sum_{i=1}^{N_c} \frac{L_i}{K_i} \right) \tag{3}$$

Evidently, the resulting displacement is the sum of those contributions from (stepped) elastic segments, as well as rotational springs. By introducing damage coefficients $\alpha$ (depending solely on the severity and locations of cracks):

$$\alpha_j = \sum_{i=1}^{N_c} \frac{L_i^j}{K_i} \tag{4}$$

geometric coefficients $\beta$ (depending solely of the non-damaged geometry of the beam):

$$\beta_j = \sum_{i=1}^{N_s} \frac{\overline{L}_i^j - \overline{L}_{i-1}^j}{j \cdot EI_i} \tag{5}$$

and their combinations:

$$\mu_j = \beta_j + \alpha_{j-1} \tag{6}$$

Eq. (3) can be rewritten in a very plain form as:

$$Y_1 = F_{n_1} \cdot \mu_3 - M_{n_1} \cdot \mu_2 \tag{7}$$

Similarly, the resulting nodal rotation $\Phi_{n_1}$ for a stepped-cantilever is also a total of those contributions from (stepped) elastic segments, as well as the rotational springs. It is expressed as:

$$\Phi_1 = -F_{n_1} \cdot \mu_2 + M_{n_1} \cdot \mu_1 \tag{8}$$

*3.1.2. Nodal transverse displacement and nodal rotation of a beam with linearly varying height*

An arbitrary variation of a cross-section's height along the axis of the element can be satisfactorily described as a stepped-beam provided that the distances of the interface between two neighbouring steps (i.e. lengths of geometric sections) are adequately selected. Although in such situations the geometric coefficients $\beta$ evaluated by Eq. (5) represents approximations of the exact values that would follow from exact integrals, these discrepancies can be neglected from the engineering point of view.

Nevertheless, beams with linearly-varying heights are hereafter studied separately, and the corresponding expressions are evaluated analytically. The cantilever utilised for the derivation of the first two columns of the beam's stiffness matrix with linearly-varying heights, is presented in Fig. 3. The linear variation of the element's height is given as $\left(\text{with abbreviations } \eta = \xi - 1 \text{ and } \xi = \frac{h_L}{h_o}\right)$:

$$h(x) = h_o \cdot \left(1 + \eta \cdot \frac{x}{L}\right)$$

where $h_o$ and $h_L$ are the beam's heights at the left and right-ends of the finite element, respectively. It should be noted that for beams with linearly-varying heights $\xi \neq 1$ and $\eta \neq 0$.

The transverse displacement $Y_1$ (equivalent of Eq. (3)) is thus given as:

$$Y_1 = F_{n_1} \cdot \left( \int_{x=0}^{L} \frac{x^2}{EI(x)} \cdot dx + \sum_{i=1}^{N_c} \frac{L_i^2}{K_i} \right) - M_{n_1} \cdot \left( \int_{x=0}^{L} \frac{x}{EI(x)} \cdot dx + \sum_{i=1}^{N_c} \frac{L_i}{K_i} \right)$$

where $EI(x)$ is the cross section's flexural rigidity as a function of coordinate $x$. When comparing the last expression to Eq. (3) it becomes apparent that the terms considering damage parameters are identical, thus demonstrating that damage coefficients $\alpha$ are independent of beam's height variation. Consequently, the last equation can be rewritten in the form of Eq. (7) by implementing already-presented damage coefficients $\alpha$ (Eq. (4)), in combination with appropriate geometric coefficients $\beta$ that correspond to beams with linearly-varying heights. These coefficients are defined by the general expression ($i = 1,2,3$):

$$\beta_i = \frac{12}{E \cdot b} \cdot \int_{x=0}^{L} \frac{x^{i-1}}{h(x)^3} \cdot dx \tag{9}$$

The separate coefficients are:

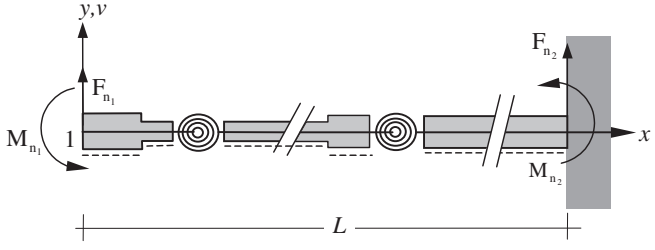


**Fig. 2.** Multi-stepped and multi-damaged cantilever, subjected to nodal force $F_{n_1}$ and bending moment $M_{n_1}$.

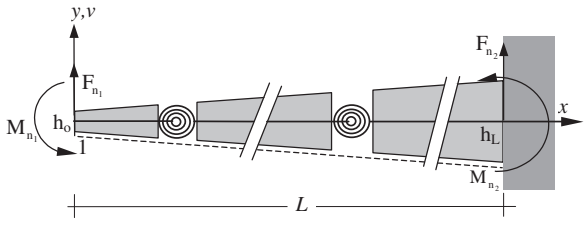


**Fig. 3.** Multi-damaged cantilever with linearly varying height, subjected to nodal force $F_{n_1}$ and bending moment $M_{n_1}$.

$$\beta_1 = \frac{L \cdot (1+\xi)}{2 \cdot EI(0) \cdot \xi^2} \tag{10}$$

$$\beta_2 = \frac{L^2}{2 \cdot EI(0) \cdot \xi^2} \tag{11}$$

$$\beta_3 = \frac{L^3 \cdot ((4-3\cdot\xi)\cdot\xi + 2\cdot\xi^2 \cdot Ln(\xi) - 1)}{2 \cdot EI(0) \cdot \eta^3 \cdot \xi^2} \tag{12}$$

It should be noted that for an element with uniform height ($\eta = 0$) Eq. (12) becomes undetermined.

The implementation of Eqs. (10)–(12), together with Eq. (4) and Eq. (6), enables the transverse displacement $Y_1$ and nodal rotation $\Phi_1$ of a cantilever with linearly-varying height to be evaluated by Eqs. (7) and (8), respectively. Consequently, these two equations allow for derivation of the coefficients of the first two columns of the stiffness matrix to be completed simultaneously for both considered structures.

### 3.1.3. Derivation of the first two columns and rows of the stiffness matrix

From these Eqs. (7) and (8), the nodal force $F_{n_1}$ and moment $M_{n_1}$ are now vice-versly expressed as functions of nodal displacement $Y_1$ and rotation $\Phi_1$:

$$F_{n_1} = \frac{\mu_1 \cdot Y_1 + \mu_2 \cdot \Phi_1}{\chi} \tag{13}$$

$$M_{n_1} = \frac{\mu_2 \cdot Y_1 + \mu_3 \cdot \Phi_1}{\chi} \tag{14}$$

with another abbreviation:

$$\chi = \mu_1 \cdot \mu_3 - \mu_2^2 \tag{15}$$

The corresponding right support's vertical reaction $F_{n_2}$ (positive upwards) due to applied loads can now be evaluated from the basic equilibrium as:

$$F_{n_2} = -F_{n_1} \tag{16}$$

whilst the corresponding reaction bending moment $M_{n_2}$ (positive anticlockwise) at the same location due to applied loads can now be evaluated as:

$$M_{n_2} = F_{n_1} \cdot L - M_{n_1} \tag{17}$$

By introducing Eqs. (13) and (14) into Eqs. (16) and (17) the reactions are also expressed by nodal displacement $Y_1$ and rotation $\Phi_1$. Consequently, since the stiffness matrix represents the relationship between nodal forces and nodal displacements, Eqs. (13), (14), (16), and (17) can be utilised to obtain the first two columns (and also the first two rows) of the stiffness matrix's considered finite element.

Therefore, by taking $\Phi_1 = 0$ in Eqs. (13), (14), (16), and (17), the coefficients of the first row and column of the stiffness matrix can be obtained, whilst the coefficients of the second row and the column are obtained by using $Y_1 = 0$.

### 3.2. Cantilever clamped at the left-end

The process of the free-end's vertical displacement and rotation calculation is now repeated for a cantilever, clamped at the left-end. This allows for the remaining third and fourth columns of the stiffness matrix to be derived at (due to its symmetry, only three coefficients are actually still unknown).

The structure is subject to a vertical upward-force $F_{n_2}$ and an anticlockwise bending moment $M_{n_2}$ at the free right-end, and the vertical displacement $Y_2$ and the rotation $\Phi_2$ of the same end are first expressed as functions of both applied loads. A virtual vertically-upward force $\delta x_3 = 1$ and a virtual anticlockwise bending moment $\delta x_4 = 1$ are thus separately applied at the free-end, in order to obtain transverse displacement and rotation of this point. The transverse displacement $Y_2$ due to both applied loads is thus obtained by integrating the bending moment diagram due to the applied transverse force $\delta x_3$ with the diagrams of moments due to loads $F_{n_2}$ and $M_{n_2}$:

$$Y_2 = F_{n_2} \cdot (\mu_3 - 2 \cdot L \cdot \mu_2 + L^2 \cdot \mu_1) + M_{n_2} \cdot (L \cdot \mu_1 - \mu_2) \tag{18}$$

In order to obtain rotation, the cantilever is further subjected to a virtual bending moment $\delta x_4$ at the right-end, and the rotation is obtained by integrating the diagram due to applied bending moment $\delta x_4$ with the diagrams of bending moments due to loads:

$$\Phi_2 = F_{n_2} \cdot (L \cdot \mu_1 - \mu_2) + M_{n_2} \cdot \mu_1 \tag{19}$$

The last two general expressions are applicable for stepped-beams as well as beams with linearly-varying heights. From these expressions the nodal force $F_{n_2}$ and the moment $M_{n_2}$ are vice versa expressed as functions of nodal displacement $Y_2$ and rotation $\Phi_2$:

$$F_{n_2} = \frac{\mu_1 \cdot Y_2 + (\mu_2 - \mu_1 \cdot L) \cdot \Phi_2}{\chi} \tag{20}$$

$$M_{n_2} = \frac{(\mu_2 - \mu_1 \cdot L) \cdot Y_2 + (\mu_3 - 2 \cdot \mu_2 \cdot L + \mu_1 \cdot L^2) \cdot \Phi_2}{\chi} \tag{21}$$

Furthermore, the reactions at the left-support, that can actually serve for verification purposes only, are:

$$F_{n_1} = -F_{n_2} \tag{22}$$

$$M_{n_1} = -M_{n_2} - F_{n2} \cdot L \tag{23}$$

By taking $Y_2 = 0$ in Eqs. (20)–(23), the remaining coefficients of the third row and the column of the stiffness matrix are obtained (to obtain the missing coefficients of the stiffness matrix Eqs. (20) and (21) are the only ones actually needed due to the symmetry of the matrix), whilst the remaining coefficients of the fourth row and the column are obtained by inserting $\Phi_2 = 0$.

Finally, the complete stiffness matrix of the multi-cracked stepped-beam's finite element (MCSBFE) is thus generally written as:

$$[K_{MCSBFE}] = \frac{1}{\chi} \cdot \begin{bmatrix} \mu_1 & \mu_2 & -\mu_1 & \mu_1 \cdot L - \mu_2 \\ \mu_2 & \mu_3 & -\mu_2 & \mu_2 \cdot L - \mu_3 \\ -\mu_1 & -\mu_2 & \mu_1 & \mu_2 - \mu_1 \cdot L \\ \mu_1 \cdot L - \mu_2 & \mu_2 \cdot L - \mu_3 & \mu_2 - \mu_1 \cdot L & \mu_1 \cdot L^2 - 2 \cdot L \cdot \mu_2 + \mu_3 \end{bmatrix} \tag{24}$$

Although this very compact form is simultaneously valid for stepped-beams as well as beams with linearly- varying heights, it should be noted that the $\beta$ coefficients involved in the evaluation of the matrix's coefficients, actually differ for both types of structure. Additionally, if a beam with an arbitrary variation of cross-sectional height along the beam's axis is adequately modelled by a sequence of steps, and the geometric coefficients $\beta$ are evaluated by Eq. (5), Eq. (24) can also be applied for such a situation.

It can be verified that, for a beam with an arbitrary number of cracks and uniform height $\left(\text{implementing } \beta_j = \frac{L^j}{j \cdot EI}\right)$ the stiffness matrix from Eq. (24), although now presented in much more compact form, reduces into the form already presented by Skrinar and Pliberšek (2012).

It should be further noted that for the case of multi-stepped beams with multiple cracks Eq. (24), although derived at in an essentially different way, produces identical results to those matrixes already presented by Biondi and Caddemi (2007).

## 4. Derivation of the load vector due to uniform load $q$ over the whole finite element

Similarly to the derivation of the stiffness matrix, the load vector's coefficients are also formally derived from separate derivations on two structures.

A cantilever clamped at the right-end and subjected to a uniformly-distributed load $q$ (positive upwards) is considered during the derivation of the load vector's first two coefficients.

The nodal transverse displacement $Y_{1,q}$ of the free-end is obtained by integrating the diagram of the bending moments for the structure subjected to the applied distributed load $q$, with the diagram for the structure subjected to the virtual vertically-upward force $\delta x_1$:

$$Y_{1,q} = \frac{q}{2} \cdot \mu_4 \tag{25}$$

For stepped-beams the geometric coefficient $\beta_4$ that appears in Eq. (25) is evaluated from Eq. (5), and for beams with linearly varying heights, the coefficient takes the form:

$$\beta_4 = \frac{L^4 \cdot (1 - 6 \cdot \xi + 3 \cdot \xi^2 + 2 \cdot \xi^3 - 6 \cdot \xi^2 \cdot Ln(\xi))}{2 \cdot EI(0) \cdot \eta^4 \cdot \xi^2} \tag{26}$$

Similarly, the nodal rotation $\Phi_{1,q}$ of the free-end is obtained by integrating the moment diagram for the structure subjected to the applied load $q$, with the diagram due to the applied virtual anticlockwise bending moment $\delta x_2 = 1$:

$$\Phi_{1,q} = -\frac{q}{2} \cdot \mu_3 \tag{27}$$

The originally distributed load is, in the finite element model, replaced by concentrated nodal forces ($F_{n_1,q}$ and $F_{n_2,q}$) and bending moments ($M_{n_1,q}$ and $M_{n_2,q}$), and the substituted loads must provide identical nodal displacement and rotation to that of the genuine one. Since the transverse nodal displacement and rotation due to force $F_{n_1}$, and moment $M_{n_1}$ are already known, Eqs. (7) and (8), respectively, the substituted nodal force and moment are obtained from a system of two linear equations:

$$\frac{q}{2} \cdot \mu_4 = F_{n_1,q} \cdot \mu_3 - M_{n_1,q} \cdot \mu_2$$

$$-\frac{q}{2} \cdot \mu_3 = -F_{n_1,q} \cdot \mu_2 + M_{n_1,q} \cdot \mu_1$$

that yield the first two coefficients of the load vector as:

$$F_{n_1,q} = \frac{q}{2} \cdot \frac{\psi}{\chi} \tag{28}$$

$$M_{n_1,q} = \frac{q}{2} \cdot \frac{\lambda}{\chi} \tag{29}$$

with abbreviations

$$\psi = \mu_1 \cdot \mu_4 - \mu_2 \cdot \mu_3 \tag{30}$$

and

$$\lambda = \mu_2 \cdot \mu_4 - \mu_3^2 \tag{31}$$

The remaining two terms of the load vector can be derived at in a similar manner from a cantilever clamped at the left-end. However, these coefficients can also be determined from a simple static equilibrium of a cantilever clamped at the right-end:

$$F_{n2,q} = \frac{q}{2} \cdot \frac{2 \cdot L \cdot \chi - \psi}{\chi} \tag{32}$$

$$M_{n2,q} = \frac{q}{2} \cdot \frac{L \cdot \psi - L^2 \cdot \chi - \lambda}{\chi} \tag{33}$$

As for the stiffness matrix it should be noted that the $\beta$ coefficients required for the evaluation of load vector's coefficients (Eqs. (28)–(33)), are different for stepped-beams than for beams with linearly-varying heights.

## 5. Computation of exact transverse displacements along the finite element

In current derivations the transverse displacements interpolation (or shape) functions were not derived at for two reasons. Firstly, they were unrequired, as the presented derivations were accomplished completely without their utilisation. Secondly, standard interpolation functions are complete polynomials of the third degree and their implementation, in those situations where either the transverse-distributed load is applied or the beams have non-uniform heights, does not produce accurate results. Therefore, the governing differential equations solutions' have to be considered in order to obtain the correct transverse displacements for both the exposed situations.

### 5.1. Mathematical form of transverse displacement's function

Generally, $N_c$ cracks and $N_s$ steps divide a stepped-beam into altogether $N_c + N_s$ elastic segments (for beams with linearly-varying heights $N_s = 1$) of various uniform heights. Every segment (excluding the first and last) is bounded either by a crack or discrete step at each end. The formal approach to transverse displacement computation thus requires the solving of $N_c + N_s$ coupled governing differential equations (GDE), thus implementing four kinematical boundary conditions and $4 \cdot (N_c + N_s - 1)$ continuity conditions.

However, the general mathematical forms of the GDE's solutions for each elastic segment of a stepped-beam or a beam with linearly-varying heights, can be obtained in advance. For the $i$th ($i = 1,2,\ldots,N_c + N_s$) elastic segment, the shear force $V_i(x)$ can be evaluated from the transverse continuous load $q(x)$ as follows:

$$V_i(x) = D_i + q^{[1]}(x) \tag{34}$$

where $q^{[m]}(x)$ denotes the $m$th anti-derivative of the transverse continuous load $q(x)$ without a constant of integration, and $D_i$ represents a constant of integration. Furthermore, $i$th segment's bending-moment $M_i(x)$ is expressed as (with $C_i$ being constants of integration):

$$M_i(x) = C_i + D_i \cdot x + q^{[2]}(x) \tag{35}$$

Eqs. (34) and (35) are applicable to both stepped-beams as well as beams with linearly varying heights.

Although rotations $\varphi_i(x)$ are obtained from bending-moments (given by Eq. (35)) for both types of considered beams, their derivations must be studied separately due to the inclusions of flexural rigidity.

#### 5.1.1. Stepped-beam

For a stepped-beam the relationship between the $\varphi_i$th segment's bending-moment $M_i(x)$ and the rotation $\varphi_i(x)$ is given as:

$$M_i(x) = EI_i \cdot \frac{d\varphi_i(x)}{dx} \tag{36}$$

where $EI_i$ is the uniform flexural rigidity of the $i$th elastic segment.

The rotations can thus be expresses as (with $b_i$ being the constants of integration):

$$\varphi_i(x) = b_i + C_i \cdot x + \frac{D_i}{2} \cdot x^2 + \frac{q^{[3]}(x)}{EI_i} \tag{37}$$

The transverse displacements $w_i(x)$ are further obtained by integrating the rotations. Therefore, the general mathematical form of the GDE's solution for each elastic segment of a stepped beam is a complete polynomial of the third degree plus $\frac{q^{[4]}(x)}{EI_i}$. It has the general form:

$$w_i(x) = a_i + b_i \cdot x + c_i \cdot x^2 + d_i \cdot x^3 + \frac{q^{[4]}(x)}{EI_i} \tag{38}$$

with four unknown coefficients (constants of integration $a_i$, $b_i$, $c_i$ and $d_i$) that must be determined either from the boundary conditions of the finite element (for $i = 1$) or the continuity conditions between two consecutive elastic segments (for $i > 1$).

*5.1.2. Beam with linearly-varying height*

Generally, $N_c$ cracks divide a beam with linearly-varying height into $N_c + 1$ elastic segments. Each segment (excluding the first and the last) is bounded by a crack at both ends. The formal approach to transverse displacement computation thus requires solving (up to) the $N_c + 1$ coupled governing differential equations (GDE), implementing four kinematical boundary conditions and $4 \cdot N_c$ continuity conditions.

However, when initiating from Eq. (35) the relationship between the segment bending moment $M_i(x)$ and the rotation $\varphi_i(x)$ for beams with linearly varying heights, is given as:

$$M_i(x) = EI(x) \cdot \frac{d\varphi_i(x)}{dx} \tag{39}$$

The rotations are thus expressed as (where $\int$ represents anti-derivative without constants of integration which is given as $B_i$):

$$\varphi_i(x) = B_i + C_i \cdot \int \frac{1}{EI(x)} \cdot dx + D_i \cdot \int \frac{x}{EI(x)} \cdot dx + \int \frac{q^{[2]}(x)}{EI(x)} \cdot dx \tag{40}$$

Finally, the general mathematical form of the GDE's solution for each elastic segment of a beam with linearly-varying height can be given as:

$$w_i(x) = A_i + B_i \cdot x + C_i \cdot \int \left( \int \frac{1}{EI(x)} \cdot dx \right) \cdot dx + D_i \cdot \int \left( \int \frac{x}{EI(x)} \cdot dx \right) \cdot dx + \int \left( \int \frac{q^{[2]}(x)}{EI(x)} \cdot dx \right) \cdot dx \tag{41}$$

or in plain general form:

$$w_i(x) = A_i + B_i \cdot x + C_i \cdot o_1(x) + D_i \cdot o_2(x) + q_4(x) \tag{42}$$

with four unknown coefficients (constants $A_i$, $B_i$, $C_i$ and $D_i$).

The first two double integrals in Eq. (41) are load-independent. The evaluation of the first yields:

$$o_1(x) = \frac{L^3}{2 \cdot EI(0) \cdot (L + x \cdot \eta) \cdot \eta^2} \tag{43}$$

Also the second double integral can be evaluated independently from the distributed load:

$$o_2(x) = -\frac{L^3 \cdot \left( \frac{L}{L + x \cdot \eta} + 2 \cdot Ln\left( \left( x + \frac{L}{\eta} \right) \cdot Sgn(\eta) \right) \right)}{2 \cdot EI(0) \cdot \eta^3} \tag{44}$$

with *Sgn* denoting the sign (or signum) function.

The last double integral of Eq. (41) is load-dependent. For frequent case $q(x) = \text{const} = q$ it obtains the following form:

$$q_4(x) = \frac{L^3 \cdot q \cdot \left( 2 \cdot (3 \cdot L + x \cdot \eta) \cdot Ln\left( \left( x + \frac{L}{\eta} \right) \cdot Sgn(\eta) \right) - L \cdot Sgn(\eta) - x \cdot \eta \cdot \left( 2 + \frac{L}{L + x \cdot \eta} \right) \right)}{4 \cdot EI(0) \cdot \eta^4} \tag{45}$$

*5.2. Derivation of coefficients for first elastic segment*

With the general expressions already known for the elastic segments of each type of considered beams, the coefficients for the first elastic segment (between the left-node and the first crack or step) can be obtained from boundary conditions rather than from the system of coupled GDE that can be transformed into a system of linear equations. The four boundary conditions consist of kinematical and mechanical conditions. Whilst the two kinematical conditions (transverse displacement $Y_1 = w_1(0)$ and rotation $\phi_1 = \phi_1(0)$) are obtained from a global stiffness matrix and a load vector of the structure, two mechanical conditions (shear force $V_1(0)$ and bending-moment $M_1(0)$) at the first element's node are afterwards obtained from the local element's stiffness matrix and load vector. These conditions allow for determining the transverse displacement's coefficients for the first elastic segment.

*5.2.1. Stepped-beam*

For a stepped-beam, each coefficient from Eq. (38) can be evaluated individually. They are given as follows:

$$a_1 = Y_1 \quad b_1 = \Phi_1 \quad c_1 = \frac{M_1(0)}{2 \cdot EI_1} \quad d_1 = \frac{V_1(0)}{6 \cdot EI_1} \tag{46}$$

*5.2.2. Beam with linearly-varying height*

For a beam with linearly-varying height the coefficients $C_1$ and $D_1$ are evaluated first. They are given as follows:

$$C_1 = M_1(0) - q^{[2]}(0) \tag{47}$$

$$D_1 = V_1(0) - q^{[1]}(0) \tag{48}$$

where the terms $q^{[2]}(0)$ and $q^{[1]}(0)$ vanish for for $q(x) = \text{const} = q$.

With known coefficients $C_1$ and $D_1$ coefficient $B_1$ follows from Eq. (40) by introducing the known rotation $\Phi_1$ at the left-node:

$$B_1 = \Phi_1 + \left( C_1 + \frac{D_1 \cdot L}{\eta} \right) \cdot \frac{L}{2 \cdot EI(0) \cdot \eta} - \int \frac{q^{[2]}(x)}{EI(x)} \cdot dx \Big|_{x=0} \tag{49}$$

The last term in Eq. (49) is load-dependent, and for $q(x) = \text{const} = q$ it obtains the form:

$$\int \frac{q^{[2]}(x)}{EI(x)} \cdot dx \Big|_{x=0} = \frac{L^3 \cdot q \cdot \left( 3 + 2 \cdot Ln\left( \frac{L}{|\eta|} \right) \right)}{4 \cdot EI(0) \cdot \eta^3} \tag{50}$$

Finally, the remaining coefficient $A_1$ is obtained from known nodal transverse displacement $Y_1$ as:

$$A_1 = Y_1 - C_1 \cdot o_1(0) - D_1 \cdot o_2(0) - q_4 \tag{51}$$

*5.3. Derivation of coefficients for consecutive elastic segments*

When the complete transverse displacement's function for the first elastic part is known, four continuity conditions allow for a determination of the unknown constants ($a_i$, $b_i$, $c_i$ and $d_i$ or $A_i$, $B_i$, $C_i$ and $D_i$, $i > 1$) for the next successive neighbouring elastic part.

*5.3.1. Stepped-beam*

General forms that relate the coefficients $c_i$ and $d_i$ ($i > 1$) of $i$th elastic section with the coefficients $c_{i-1}$ and $d_{i-1}$ of the preceding neighbouring elastic section $i - 1$, do not depend on the type of connection between sections (crack or discrete change of cross section):

$$c_i = c_{i-1} \cdot \frac{EI_{i-1}}{EI_i} \tag{52}$$

$$d_i = d_{i-1} \cdot \frac{EI_{i-1}}{EI_i} \tag{53}$$

It is further evident from Eqs. (52) and (53) that for a crack the expressions reduce into $c_i = c_{i-1}$ and $d_i = d_{i-1}$.

However, the relationships between the coefficients $a_i$ and $b_i$ ($i > 1$) of $i$th elastic section and the coefficients $a_{i-1}$ and $b_{i-1}$ of the preceding neighbouring elastic segment depend on the type of connection (crack or discrete change of cross section) between the segments.

If a crack with rotational spring $K_j$ separates elastic sections $i-1$ and $i$ at distance $L_j$ the relationships are given as (considering $EI_i = EI_{i-1}$):

$$b_i = b_{i-1} + \frac{2 \cdot c_{i-1} \cdot EI_i + 6 \cdot d_{i-1} \cdot EI_i \cdot L_j + q^{[2]}(L_j)}{K_j} \tag{54}$$

$$a_i = a_{i-1} - \frac{2 \cdot EI_i \cdot L_j \cdot (c_{i-1} + 3 \cdot L_j \cdot d_{i-1}) + L_j \cdot q^{[2]}(L_j)}{K_j} \tag{55}$$

For a discrete-step-change of the cross-section at distance $\bar{L}_j$ the relationships are given as:

$$b_i = b_{i-1} + 2 \cdot (c_{i-1} - c_i) \cdot \bar{L}_j + 3 \cdot (d_{i-1} - d_i) \cdot \bar{L}_j^2 + \frac{q^{[3]}(\bar{L}_j)}{EI_{i-1}} - \frac{q^{[3]}(\bar{L}_j)}{EI_i} \tag{56}$$

$$a_i = a_{i-1} + (c_i - c_{i-1}) \cdot \bar{L}_j^2 + 2 \cdot (d_i - d_{i-1}) \cdot \bar{L}_j^3 + \frac{q^{[4]}(\bar{L}_j)}{EI_{i-1}} - \frac{q^{[4]}(\bar{L}_j)}{EI_i} - \frac{\bar{L}_j \cdot q^{[3]}(\bar{L}_j)}{EI_{i-1}} + \frac{\bar{L}_j \cdot q^{[3]}(\bar{L}_j)}{EI_i} \tag{57}$$

*5.3.2. Beam with linearly-varying height*

If follows from the equivalences of the shear forces and bending moments at the crack location $L_i$ between the elastic sections $i-1$ and $i$ that:

$$D_i = D_{i-1} \tag{58}$$

$$C_i = C_{i-1} \tag{59}$$

and, consequently, the relationships can be written as $D_i \equiv D_1 \equiv D$ and $C_i \equiv C_1 \equiv C$.

The continuity condition for rotations further yields:

$$B_i = B_{i-1} + \frac{C + D \cdot L_{i-1} + q^{[2]}(L_{i-1})}{K_{i-1}} \tag{60}$$

Finally, the continuity condition for transverse displacements yields:

$$A_i = A_{i-1} + (B_{i-1} - B_i) \cdot L_{i-1} \tag{61}$$

This procedure, during which all elastic sections' coefficients can be easily evaluated solely from its boundary conditions, is afterwards repeated in sequence towards the last elastic part. The exact transverse displacements of the complete finite-element are thus obtained by basic mathematical operations, and neither the explicit solving of coupled GDEs nor the solving of $N_c + N_s$ systems of linear equations with four unknowns, are required.

## 6. Numerical applications

The applicability of derived at expressions for stiffness matrix, load vector, and transverse displacements' functions is demonstrated in three examples. The relevance of the discussed expression is confirmed by comparing the obtained results for transverse displacements and the reactions at the supports to the results from alternative 2D finite element models.

*6.1. Example 1 – stepped multi-cracked beam*

In first example, a 9 m long stepped multi-cracked beam was analyzed. The beam under consideration had three stepped segments with piecewise constant rectangular cross-sections' dimensions, Fig. 4. The Young modulus of the material was $E = 30$ GPa with Poisson's ratio 0.3. Three cracks were introduced, located at distances of 2 m, 4 m and 7.5 m from the left-end. The relative crack-depth was taken to be $\delta = 0.5$ m for all cracks, as identical relative depths minimize the influence of the rotational spring-stiffness definition on the results. The genuine definition given by Okamura was selected from among all existing definitions for rotational spring due to the fact that it is the only one that takes Poisson's ratio into account. For the relative crack-depth of $\delta = 0.5$ this definition also produces results which have been proved to be in good agreement with those experimentally obtained values, as presented by Vestroni (2009). The analysed beam was loaded with a downward transverse uniform load $q = 1$ kN/m along the whole element and three different combinations of boundary conditions were studied. The computational model for all three structures consisted of a single presented beam finite-element with just two nodes, thus representing the smallest possible finite-element computational model.

The stiffness matrix of the single multicracked stepped beam finite element (MCSBFE) was obtained from Eq. (24):

$$[\mathbf{K}_1] = \begin{bmatrix} 64915.1096 & 312673.5571 & -64915.1096 & 271562.4296 \\ 312673.5571 & 1802260.5914 & -312673.5571 & 1011801.4224 \\ -64915.1096 & -312673.5571 & 64915.1096 & -271562.4296 \\ 271562.4296 & 1011801.4224 & -271562.4296 & 1432260.4442 \end{bmatrix}$$

The model had four degrees of freedom but by considering known displacements or rotations at the boundaries of the structure, the discrete unknowns (vertical displacement and rotations) at the nodes for all considered situations were evaluated from systems of up to two linear equations.

*6.1.1. Simply supported beam*

The stiffness matrix of the simply supported beam was obtained by eliminating the first and third columns and rows of the element's stiffness matrix:

$$[K_{ss}] = \begin{bmatrix} 1802260.5914 & 1011801.4224 \\ 1011801.4224 & 1432260.4442 \end{bmatrix}$$

The unknown nodal rotations of both ends were thus obtained by implementing the corresponding load vector obtained from Eqs. (29) and (33):

$$\{F\} = \begin{Bmatrix} -9229.15419 \text{ Nm} \\ 6546.1719 \text{ Nm} \end{Bmatrix}$$

The vertical reactions/nodal shear-forces at both ends were further evaluated over the element's stiffness matrix and nodal rotations.

Since three cracks were introduced within three constant geometric sections of the structure, six functions for six elastic regions altogether had to be analysed in order to obtain vertical displacement distributions along the structure. Due to a distributed load that was applied to the structure, each region's interpolation function following on from Eq. (38) was a complete polynomial of the

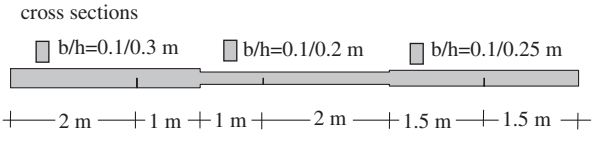


**Fig. 4.** First example structural setup.

fourth degree. The following function for transverse displacements between left node and first crack was obtained by the implementation of the boundary conditions for the left-end, into Eq. (46):

$$w_1(x) = -1.27391 \cdot 10^{-2} \cdot x + 1.11111 \cdot 10^{-4} \cdot x^3 - 6.17284 \cdot 10^{-6} \cdot x^4 \quad 0 \leqslant x \leqslant 2\ \text{m}$$

The remaining functions for transverse displacements were further obtained by the implementation of continuity conditions at discrete steps and cracks, Eqs. (52)–(57):

$$w_2(x) = -1.98035 \cdot 10^{-3} - 1.17489 \cdot 10^{-2} \cdot x + 1.11111 \cdot 10^{-4} \cdot x^3 - 6.17284 \cdot 10^{-6} \cdot x^4 \quad 2\ \text{m} \leqslant x \leqslant 3\ \text{m}$$

$$w_3(x) = 8.70715 \cdot 10^{-3} - 1.72906 \cdot 10^{-2} \cdot x + 3.75 \cdot 10^{-4} \cdot x^3 - 2.08333 \cdot 10^{-5} \cdot x^4 \quad 3\ \text{m} \leqslant x \leqslant 4\ \text{m}$$

$$w_4(x) = -4.0237 \cdot 10^{-3} - 1.41079 \cdot 10^{-2} \cdot x + 3.75 \cdot 10^{-4} \cdot x^3 - 2.08333 \cdot 10^{-5} \cdot x^4 \quad 4\ \text{m} \leqslant x \leqslant 6\ \text{m}$$

$$w_5(x) = -4.35517 \cdot 10^{-2} - 3.12789 \cdot 10^{-3} \cdot x + 1.92 \cdot 10^{-4} \cdot x^3 - 1.06667 \cdot 10^{-5} \cdot x^4 \quad 6\ \text{m} \leqslant x \leqslant 7.5\ \text{m}$$

$$w_6(x) = -5.2145 \cdot 10^{-2} - 1.98211 \cdot 10^{-3} \cdot x + 1.92 \cdot 10^{-4} \cdot x^3 - 1.06667 \cdot 10^{-5} \cdot x^4 \quad 7.5\ \text{m} \leqslant x \leqslant 9\ \text{m}$$

The remaining unused four boundary conditions at the right-end served for verification purposes only.

The considered structure was furthermore modelled through 2D plane finite elements by implementing the COSMOS/M finite element program. In similar 2D FE models where crack propagation has been studied the mesh-density increased within the vicinity of a crack, and crack-tip stress singularity was commonly modelled by eight singular triangular elements placed around the crack-tip (Sadowski et al., 2009). However, since in the considered example non-propagation of cracks was assumed, uniform quadrilateral elements were implemented. The transverse displacements and reactions were obtained from a computational model consisting of 22,500 2D eight noded rectangular elements with almost 70,000 nodal points. In each node, two degrees of freedom were taken into account – vertical and horizontal displacements. Vertical and horizontal displacements were obtained in discrete points by solving approximately 140,000 linear equations.

The results for several significant discrete parameters (transverse displacements, rotations and reactions) from both applied computational models were compared and are summarized in Table 1. The table shows that the MCSBFE's values for vertical reactions in the supports are identical to the values from the basic static analysis. Furthermore, it is evident from the table that the displacement discrepancies at the elements' steps are smaller than those at the cracks. Furthermore, the cracks' discrepancies are somewhat higher for both cracks closer to the supports. Nevertheless, the matching of the results is very good. The maximum discrepancy of the displacements (appearing at the location of third crack) is slightly smaller than 1.5%, and the error at maximum displacement's location is slightly smaller than 0.75%.

The comparison between transverse displacements along the axis obtained by both implemented approaches is given in Fig. 5, where only very small discrepancies are noticeable (the results from MCSBFE are slightly higher than those from the 2D plane finite elements model).

**Table 1**
Comparison of the results from two different computational approaches.

| Parameter | MCSBFE | COSMOS/M 22,500 2D FE |
|---|---|---|
| Vertical reaction at the left support (A) | 4500 N | 4500 N |
| Rotation at the left support (A) | $-1.2739 \cdot 10^{-2}$ rad | $-1.265 \cdot 10^{-2}$ rad[a] |
| Vertical reaction at the right support (B) | 4500 N | 4500 N |
| Rotation at the right support (B) | $1.3570 \cdot 10^{-2}$ rad | $1.3393 \cdot 10^{-2}$ rad* |
| Displacement at the first crack location ($x$ = 2 m) | −24.688 mm | −24.436 mm |
| Displacement at first step ($x$ = 3 m) | −34.727 mm | −34.511 mm |
| Displacement at the second crack location ($x$ = 4 m) | −41.789 mm | −41.477 mm |
| Max. displacement | −41.995 mm ($x$ = 4.287 m) | −41.691 mm ($x$ = 4.295 m) |
| Displacement at second step ($x$ = 6 m) | −34.671 mm | −34.434 mm |
| Displacement at the third crack location ($x$ = 7.5 m) | −19.761 mm | −19.474 mm |

[a] Not computed directly but evaluated from displacements of neighbouring nodes.

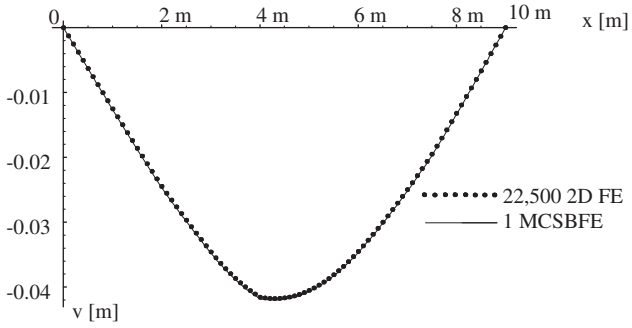


**Fig. 5.** Comparison of transverse displacements from both applied models.

*6.1.2. Propped cantilever*

This structure was obtained by fully clamping the left-end of the element from the previous case. By considering zero rotation at the left-node, as well as zero transverse displacements at both ends, the discrete value of the rotation $_2$ at the right-node was evaluated from a single linear equation:

$$1432260.4442 \cdot \Phi_2 = 6546.1719$$

This single value allowed for the computation of nodal vertical reaction forces and bending moment as well as the distribution of transverse displacements along the longitudinal axis of the structure. In addition, also this example was analyzed implementing the computational model with 22,500 2D quadrilateral plane finite elements. Fig. 6 thus represents the distribution of transverse displacements from both computations. Furthermore, the discrete values of some representative quantities are summarized in Table 2.

It is evident from Table 2 that the implementation of GDE solutions (in the form of Eq. (38)) reflects an obvious agreement of the results, as the absolute maximum difference in displacement – appearing at the third crack – is smaller than 1.3%. The difference at the maximum displacement's location is smaller than 0.6%. Except for the first crack, the results from MCSBFE slightly overvalue those from the 2D FE model.

For the vertical reactions, the maximum difference is smaller than 0.10%, whilst the difference for bending-moment in the left-support is smaller than 0.15%.

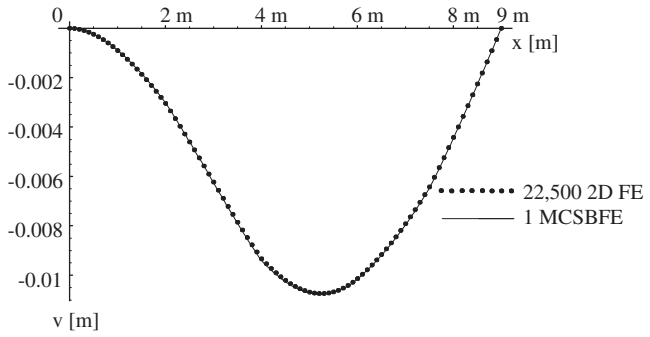


**Fig. 6.** Comparison of transverse displacements from both applied models.

**Table 2**
Comparison of results for the second case using two different computational approaches.

| Parameter | MCSBFE | COSMOS/M 22,500 2D FE |
|---|---|---|
| Vertical reaction at the left support | 6039.290 N | 6037.286 N |
| Bending moment at the left support | 13853.611 Nm | 13833.495 Nm |
| Vertical reaction at the right support | 2960.710 N | 2963.000 N |
| Rotation at the right support | $4.5705 \cdot 10^{-3}$ rad | $4.533 \cdot 10^{-3}$ rad[a] |
| Displacement at the first crack location ($x = 2$ m) | −3.011 mm | −3.032 mm |
| Displacement at first step ($x = 3$ m) | −6.244 mm | −6.208 mm |
| Displacement at the second crack location ($x = 4$ m) | −9.402 mm | −9.308 mm |
| Max. displacement | −10.771 mm ($x = 5.233$ m) | −10.710 mm ($x = 5.245$ m) |
| Displacement at second step ($x = 6$ m) | −10.152 mm | −10.103 mm |
| Displacement at the third crack location ($x = 7.5$ m) | −6.483 mm | −6.402 mm |

[a] Not computed directly but evaluated from displacements of neighbouring nodes.

### 6.1.3. Cantilever, clamped at left-end

The stiffness matrix of the cantilever, clamped at left-end was obtained by eliminating the first and second columns and rows of the element's stiffness matrix:

$$[K_c] = \begin{bmatrix} 64915.1096 & -271562.4296 \\ -271562.4296 & 1432260.4442 \end{bmatrix}$$

The unknown nodal transverse displacement and rotation of free end were thus obtained by implementing the load vector:

$$\{F\} = \begin{Bmatrix} -4201.8909\ \text{N} \\ 6546.1719\ \text{Nm} \end{Bmatrix}$$

The reactions at the clamped end were further evaluated over the element's stiffness matrix and free-end nodal transverse displacement and rotation.

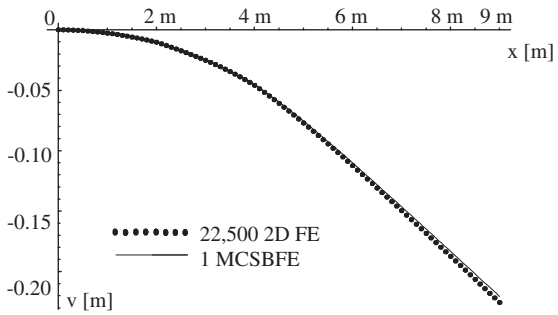


**Fig. 7.** Comparison of transverse displacements from both applied models.

As in previous cases, this example was also analysed by implementing the computational model with 22,500 2D quadrilateral plane finite elements, and Fig. 7 represents the distribution of transverse displacements from both computations. Furthermore, the discrete values of some representative quantities are summarized in Table 3.

It is evident from Fig. 7, as well as from Table 3, that the differences in the displacement's increase from clamped left-end towards the free-end. At the right-end the maximum differences appear for displacement as well as rotation (2.258% and 2.257%, respectively). Although these discrepancies appear to be slightly higher than those for the previous two cases, it should be noted that 1.029% and 1.108% errors already appear for the non-cracked structure when comparing maximal displacements and rotations, respectively. It should be additionally noted that the differences in MCSBFE's results against 2D results nonlinearly increases from the left-end. The error at the first crack (where displacement is unaffected by the cracks) is just 0.18%, whilst at the first step's displacement (which is already influenced by the first crack) the discrepancy had already increases to 1.25%. This indicates that the results in this example are very sensible for the rotational spring's stiffness.

### 6.2. Example 2 – cracked cantilever with linearly-varying height

In the second example, a multicracked cantilever beam with linearly-varying height of length $L = 8$ m was considered, Fig. 8.

The material properties were taken as $E = 30$ GPa and = 0.1. The cross-section was a rectangle with width $b = 0.1$ m where the height h was linearly decreasing from $h = 0.6$ m at the left-end to $h = 0.3$ m at the right-end.

Three transverse cracks were located at distances 2 m, 4 m and 6 m from the left, clamped end. As in first example, just in order to avoid discussion about the rotational stiffness definition and to minimize its influence on the results, the relative crack depth of 0.5 was considered for all cracks. Further, Okamura's definition was once more utilised for the rotational spring stiffness evaluation.

The stiffness matrix of the single MCSBFE was obtained from Eq. (24) by implementing the corresponding geometric coefficients $\beta$, Eqs. (10)–(12):

$$[\mathbf{K}_1] = \begin{bmatrix} 373696.7225 & 1884013.4001 & -373696.7225 & 1105560.3798 \\ 1884013.4001 & 11009897.9066 & -1884013.4001 & 4062209.2942 \\ -373696.7225 & -1884013.4001 & 373696.7225 & -1105560.3798 \\ 1105560.3798 & 4062209.2942 & -1105560.3798 & 4782273.7439 \end{bmatrix}$$

**Table 3**
Comparison of results for the third case using different computational approaches.

| Parameter | MCSBFE | COSMOS/M 22,500 2D FE |
|---|---|---|
| Vertical reaction at the left support (A) | 9000 N | 9001.24 N |
| Bending moment at the left support (A) | 40500 Nm | 40502 Nm |
| Displacement at the first crack location ($x = 2$ m) | −10.321 mm | −10.3400 mm |
| Displacement at first step ($x = 3$ m) | −24.966 mm | −25.282 mm |
| Displacement at the second crack location ($x = 4$ m) | −45.119 mm | −45.988 mm |
| Displacement at second step ($x = 6$ m) | −110.007 mm | −112.540 mm |
| Displacement at the third crack location ($x = 7.5$ m) | −164.716 mm | −168.530 mm |
| Displacement at the right end | −220.525 mm | −225.620 mm |
| Rotation at the right end | $-3.7242 \cdot 10^{-2}$ rad | $-3.81 \cdot 10^{-2}$ rad[a] |

[a] Not computed directly but evaluated from displacements of neighbouring nodes.

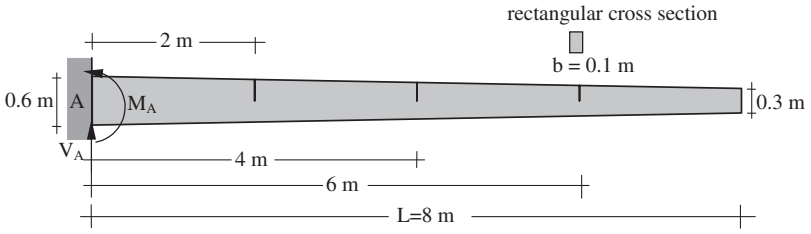


**Fig. 8.** The second example setup.

Two load cases were analysed: the vertical concentrated downward force $F$ at the free-end and the vertical uniform continuous downward load $q$ over the whole length.

By considering the boundary conditions at the left-node, the discrete value of the displacement and rotation were evaluated at the right-node using a system of two linear equations:

$$\begin{bmatrix} 373696.7225 & -1105560.3798 \\ -1105560.3798 & 4782273.7439 \end{bmatrix} \cdot \begin{Bmatrix} u_2 \\ \Phi_2 \end{Bmatrix} = \{F\}$$

where {F} represents the load case's corresponding load vector.

*6.2.1. First load case – vertically concentrated downward force F*

In the first load case the structure was loaded by a vertical downward force 1000 N at the free-end. The load corresponding load vector could be established directly and had the following form:

$$\{F\} = \begin{Bmatrix} -1000\ \mathrm{N} \\ 0 \end{Bmatrix}$$

The obtained discrete values of vertical displacement and rotation of the free end further allowed for the computation of nodal vertical reaction force and bending moment of the clamped-end as well as the distribution of transverse displacements along the longitudinal axis of the structure.

The structure had three cracks. Consequently, four elastic regions had to be analysed in order to obtain vertical displacements' distribution along the structure. The complete cantilever was thus divided into four elastic segments (each of 2 m length). The transverse displacements functions for each elastic region were obtained in the form of Eq. (42), with the following terms:

$$o_1(x) = -\frac{3.7925926 \cdot 10^{-5}}{x - 16}$$

$$o_2(x) = \frac{6.0681481 \cdot 10^{-4}}{16 - x} + 7.5851852 \cdot 10^{-5} \cdot Ln(16 - x)$$

$$q_4(x) = 0$$

Furthermore, to complete the transverse displacements functions 10 coefficients ($C$, $D$, $A_i$ and $B_i$, $i = 1,\ldots,4$) remained to be obtained.

Known values for bending moment and shear force at the left-node initially allowed for the determination of coefficients $C$ and $D$ from Eqs. (49) and (51), respectively. Since $D_i \equiv D$ and $C_i \equiv C$ these two values were further valid for all remaining segments.

Afterwards, known nodal rotation and displacement at the left-node further allowed for the determination of coefficients $B_1$ and $A_1$ from Eqs. (58) and (59), respectively. Further by implementing Eqs. (60) and (61) the remaining coefficients $A_i$ and $B_i$ were sequentially evaluated for the second and also all further segments, in a very straightforward manner. All the calculated coefficients are given in Table 4.

This structure was also analysed by implementing the COSMOS/M finite element program. The computational model consisted of 14,400 2D quadrilateral plane finite elements with almost 45,000 nodal points. In each node, two degrees of freedom were taken into account – vertical and horizontal displacements. The model's vertical and horizontal displacements were obtained in discrete points by solving approximately 90,000 linear equations.

**Table 4**
The coefficients required for calculating the stiffness matrix and transverse displacements.

| Coefficient | Value | Coefficient | Value |
|---|---|---|---|
| $\alpha_o$ | $2.171339814 \cdot 10^{-7}$ | $\alpha_1$ | $9.650151029 \cdot 10^{-7}$ |
| $\alpha_2$ | $4.840932046 \cdot 10^{-6}$ | $\alpha_3$ | $2.605295113 \cdot 10^{-5}$ |
| $\beta_1$ | $4.444444444 \cdot 10^{-7}$ | $\beta_2$ | $2.370370370 \cdot 10^{-6}$ |
| $\beta_3$ | $1.465057133 \cdot 10^{-5}$ | $\beta_4$ | $9.641260881 \cdot 10^{-5}$ |
| $C$ | −8000 | $D$ | 10000 |
| $B_1$ | $-3.5555556 \cdot 10^{-3}$ | $A_1$ | −0.2292690 |
| $B_2$ | $3.25405812 \cdot 10^{-3}$ | $A_2$ | −0.2286660 |
| $B_3$ | $2.9804771 \cdot 10^{-3}$ | $A_3$ | −0.2275716 |
| $B_4$ | $2.7834988 \cdot 10^{-3}$ | $A_4$ | −0.2263898 |

Fig. 9 thus represents the distribution of transverse displacements from both analysis. Furthermore, the discrete values of some representative quantities are summarized in Table 5.

It is evident from Fig. 9 that the implementation of GDE solutions (in the form of Eq. (42)) reflects an excellent agreement of the results, as no discrepancies are visually detectable. The absolute difference for displacement increases according to the distance from the clamped-end. The maximum difference which appears at the free-end is about 0.31%, whilst the difference at first crack is about 0.18%.

The considered cantilever was further modelled as a stepped-beam implementing various distances of the interface between two neighbouring steps. The geometric coefficients $\beta$ were evaluated by the genuine Eq. (5), thus representing approximations of the exact values that would follow from exact integrals (Eqs. (10)–(12) and (26)). This study was accomplished for two reasons. The first, and also the main reason, was that in this way the partic-

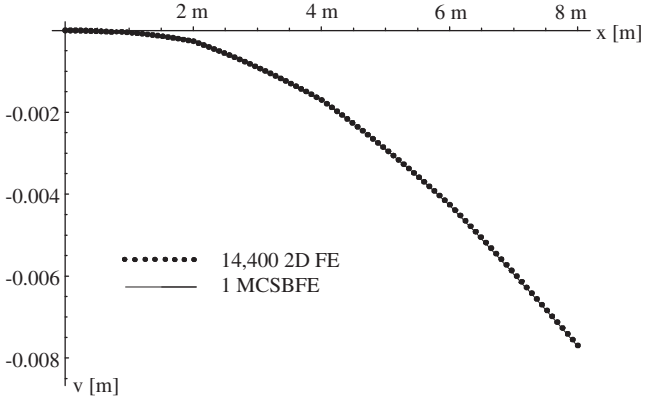


**Fig. 9.** Comparison of transverse displacements from both applied models.

**Table 5**
Comparison of the results for the second example's first load case using different computational approaches.

| Parameter | MCSBFE | COSMOS/M 14,400 2D FE |
|---|---|---|
| Vertical reaction at the left support (A) | 1000 N | 1000.13 N |
| Bending moment at the left support (A) | 8000 Nm | 7999.79 Nm |
| Displacement at the first crack location ($x = 2$ m) | −0.3085 mm | −0.3080 mm |
| Displacement at the second crack location ($x = 4$ m) | −1.881 mm | −1.877 mm |
| Displacement at the third crack location ($x = 6$ m) | −4.693 mm | −4.679 mm |
| Displacement at the right end | −8.466 mm | −8.440 mm |
| Rotation at the right end | $-1.9572 \cdot 10^{-3}$ rad | $-1.9507 \cdot 10^{-3}$ rad[a] |

[a] Not computed directly but evaluated from displacements of neighbouring nodes.

ularly derived expressions for the geometric coefficients $\beta$ were indirectly verified. The second reason was to demonstrate that in such models the discrepancies of the results can be neglected from the engineering point of view if the lengths of geometric sections are adequately selected. Therefore, Table 6 summarises the results from several situations differing in the number of geometric sections. In each presented situation, the cantilever was divided into segments of equal length.

It is clear from Table 6 that the convergence of all results (coefficients $\beta$ as well as of the displacement at the right, free end) is obvious. It is further clear that the results converge towards the results obtained by implementing exact analytical expressions for $\beta$ coefficients. The discrepancy against exact results evidently decreases simultaneously with any increase in the segments' number. Thus, by solely implementing 3 segments the error decreases below 3%, whilst the implementation of 5 segments yields an error just slightly higher than 1%. In conclusion, by implementing 10 or more segments the discrepancy obtained is 0.257% or less, which can already be neglected from the engineering point of view.

There is an additional significance apparent from the table. A very detailed approximation with short step lengths (less than 1 mm) namely shows that the solutions are numerically stable even when the distance between the two consecutive steps is diminishing.

### 6.2.2. Second load case – vertical uniform continuous downward load $q$

In the second load case the structure was loaded by a downward vertical uniform load $q = 1000$ N/m along the complete structure. The load vector for this load case was obtained (from Eqs. (32) and (33)) in the following form:

$$\{F\} = \begin{Bmatrix} -3478.637587\ \text{N} \\ 3892.747600\ \text{Nm} \end{Bmatrix}$$

It allowed for evaluating the discrete value of the vertical displacement and rotation of the free-end. The element's stiffness matrix and the vector of nodal displacements and rotations further allowed for evaluation of nodal forces and moments and, consequently, the reactions at clamped end. These values additionally allowed for evaluation of transverse displacements between the nodes.

The structure had three cracks and, consequently, four elastic segments had to be analysed in order to acquire vertical displacements' distribution along the structure. Due to the presence of continuous load in this load case the term $q_4(x)$ in Eq. (42) had to be reevaluated and then obtained the form:

$$q_4(x) = -3.7925926 \cdot 10^{-2} \cdot x - 1.8204444 \cdot Ln(16 - x) + \frac{4.8545185 + 3.7925926 \cdot 10^{-2} \cdot (16 \cdot x + x^2) \cdot Ln(16 - x)}{x - 16}$$

Furthermore, for the complete structure 10 coefficients ($C$, $D$, $A_i$ and $B_i$, $i = 1,\ldots,4$) remained to be obtained.

Known values for bending moment and shear force at the left-node allowed for the determination of coefficients $C$ and $D$, respectively.

After that, known nodal rotation and displacement at the left-node further allowed for the determination of coefficients $B_1$ and $A_1$, respectively. Further, by implementing Eqs. (60) and (61) the remaining coefficients $A_i$ and $B_i$ were sequentially evaluated for the second and also all further segments. All the calculated coefficients are given in Table 7.

The distributions of transverse displacements from both computational models are compared in Fig. 10. Furthermore, the discrete values of some representative quantities are summarized in Table 8. It is apparent from Fig. 10 and also Table 8 that the simplified model produces excellent results also for the distributed load.

**Table 7**
The coefficients required for calculating of transverse displacements.

| Coefficient | Value | Coefficient | Value |
|---|---|---|---|
| $C$ | −32000 | $D$ | 8000 |
| $B_1$ | −0.1383382 | $A_1$ | 3.4407477 |
| $B_2$ | −0.1392427 | $A_2$ | 3.4425566 |
| $B_3$ | −0.1397898 | $A_3$ | 3.4447453 |
| $B_4$ | −0.1399868 | $A_4$ | 3.4459272 |

**Table 6**
Convergence of the coefficients $\beta$ and displacement at the right end.

| $n$ | $\beta_1$ | $\beta_2$ | $\beta_3$ | $\beta_4$ | Displacement |
|---|---|---|---|---|---|
| 1 | $3.511659808 \cdot 10^{-7}$ | $1.404663923 \cdot 10^{-6}$ | $7.491540924 \cdot 10^{-5}$ | $4.494924554 \cdot 10^{-5}$ | −10.7888 mm |
| 2 | $4.139786200 \cdot 10^{-7}$ | $2.041586870 \cdot 10^{-6}$ | $1.191692301 \cdot 10^{-5}$ | $7.458691718 \cdot 10^{-5}$ | −9.0434 mm |
| 3 | $4.299527517 \cdot 10^{-7}$ | $2.212272425 \cdot 10^{-6}$ | $1.329877055 \cdot 10^{-5}$ | $8.529058107 \cdot 10^{-5}$ | −8.7167 mm |
| 4 | $4.360752311 \cdot 10^{-7}$ | $2.278675114 \cdot 10^{-6}$ | $1.385801169 \cdot 10^{-5}$ | $8.981287673 \cdot 10^{-5}$ | −8.6053 mm |
| 5 | $4.390193077 \cdot 10^{-7}$ | $2.310807013 \cdot 10^{-6}$ | $1.413303354 \cdot 10^{-5}$ | $9.207745201 \cdot 10^{-5}$ | −8.5546 mm |
| 10 | $4.430639689 \cdot 10^{-7}$ | $2.355169766 \cdot 10^{-6}$ | $1.451753166 \cdot 10^{-5}$ | $9.528892477 \cdot 10^{-5}$ | −8.4882 mm |
| 20 | $4.440977524 \cdot 10^{-7}$ | $2.366550022 \cdot 10^{-6}$ | $1.461707195 \cdot 10^{-5}$ | $9.612905526 \cdot 10^{-5}$ | −8.4718 mm |
| 50 | $4.443889025 \cdot 10^{-7}$ | $2.369758200 \cdot 10^{-6}$ | $1.464520056 \cdot 10^{-5}$ | $9.636712058 \cdot 10^{-5}$ | −8.4672 mm |
| 100 | $4.444305564 \cdot 10^{-7}$ | $2.370217295 \cdot 10^{-6}$ | $1.464922825 \cdot 10^{-5}$ | $9.640123246 \cdot 10^{-5}$ | −8.4666 mm |
| 500 | $4.444438889 \cdot 10^{-7}$ | $2.370364247 \cdot 10^{-6}$ | $1.465051760 \cdot 10^{-5}$ | $9.641215370 \cdot 10^{-5}$ | −8.4664 mm |
| 1000 | $4.444443056 \cdot 10^{-7}$ | $2.370368840 \cdot 10^{-6}$ | $1.465055789 \cdot 10^{-5}$ | $9.641249503 \cdot 10^{-5}$ | −8.4664 mm |
| 2000 | $4.444444097 \cdot 10^{-7}$ | $2.370369988 \cdot 10^{-6}$ | $1.465056797 \cdot 10^{-5}$ | $9.641258036 \cdot 10^{-5}$ | −8.4664 mm |
| 5000 | $4.444444389 \cdot 10^{-7}$ | $2.370370309 \cdot 10^{-6}$ | $1.465057079 \cdot 10^{-5}$ | $9.641260426 \cdot 10^{-5}$ | −8.4664 mm |
| 10000 | $4.444444431 \cdot 10^{-7}$ | $2.370370355 \cdot 10^{-6}$ | $1.465057119 \cdot 10^{-5}$ | $9.641260767 \cdot 10^{-5}$ | −8.4664 mm |

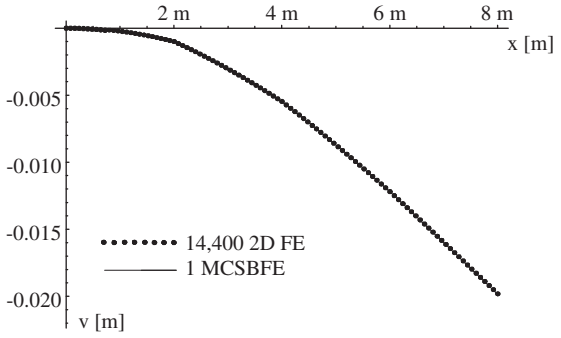


**Fig. 10.** Comparison of transverse displacements from both applied models.

**Table 8**
Comparison of the results for the second example's second load case using different computational approaches.

| Parameter | MCSBFE | COSMOS/M 14,400 2D FE |
|---|---|---|
| Vertical reaction at the left support (A) | 8000 N | 8001.785 N |
| Bending moment at the left support (A) | 32000 Nm | 32004.998 Nm |
| Displacement at the first crack location ($x = 2$ m) | −1.129 mm | −1.141 mm |
| Displacement at the second crack location ($x = 4$ m) | −6.040 mm | −6.052 mm |
| Displacement at the third crack location ($x = 6$ m) | −13.432 mm | −13.424 mm |
| Displacement at the right end | −21.832 mm | −21.791 mm |
| Rotation at the right end | $-4.2332 \cdot 10^{-3}$ rad | $-4.2123 \cdot 10^{-3}$ rad[a] |

[a] Not computed directly but evaluated from displacements of neighbouring nodes.

Although the absolute differences for displacements are comparable to those for the concentrated load's case, the maximum difference (which appears at the first crack) is 1.03% which is slightly higher (whilst the difference at maximal displacement is about 0.19%).

### 6.3. Example 3 – simple cracked-frame structures

In the third example, three multi-cracked 1 bay frames were considered. The frames studied differed not only in the geometries of the columns but also in the locations of cracks. The material properties were taken as $E = 30$ GPa, $= 0.3$, whilst the cross-sectional width was $b = 0.1$. The load for each frame consisted of two horizontal forces $F = 5000$ N.

Each frame structure was analyzed using three different computational models. The first model consisted of three beam finite elements. The non-cracked horizontal beam was modelled by standard Euler–Bernoulli beam finite element, whilst the columns were modeled either as multi-stepped elements or elements with linearly-varying heights. This model thus represents the smallest computational model as only three finite elements were utilised. The second computational model solely consisted of standard Euler–Bernoulli beam finite elements (with a single crack where required). Whilst for the multi-stepped columns the number of beam finite elements was equal to the number of steps, the columns with linearly-varying heights were modelled by a series of finite elements of uniform heights in order to simulate the actual variation of height. The last model consisted of 2D quadrilateral plane finite elements implementing the COSMOS/M finite element program.

**Table 9**
Comparison of the representative values for first frame structure.

| Parameter | MCSBFE's | Standard FEs | COSMOS/M |
|---|---|---|---|
| No. elements | 3 | 8 | 16980 |
| No. nodes | 4 | 9 | 52961 |
| No. equations | 6 | 21 | 105770 |
| Displacement $u_B$ | 9.700 mm | 9.703 mm | 9.830 mm |
| Displacement $u_C$ | 9.712 mm | 9.712 mm | 9.841 mm |
| Force $H_A$ | 6792.303 N | 6792.336 N | 6771.320 N |
| Moment $M_A$ | 11532.497 Nm | 11532.655 Nm | 11360.490 N |
| Force $H_D$ | 3207.697 N | 3207.664 N | 3228.630 N |
| Moment $M_D$ | 3768.863 Nm | 3768.863 Nm | 3798.107 N |

#### 6.3.1. First frame structure – two multi-stepped columns

The first frame structure consisted of two different multi-stepped columns with seven cracks altogether, each with 0.5 relative depths (Fig. 11). In both beam finite-element models, the columns were assumed to be of 2.5 m in length, whilst the adopted length for the beam was 4.175 m. The model's data (number of finite elements, number of nodes, number of equations), as well as some representative results (horizontal displacements of beam's ends and the reactions at the supports) are summarised in Table 9.

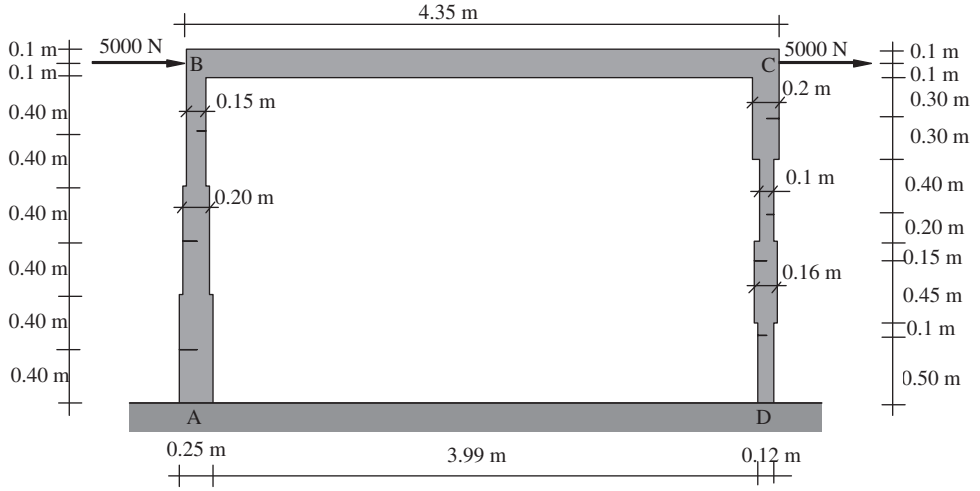


**Fig. 11.** Frame structure with two multi-stepped columns.

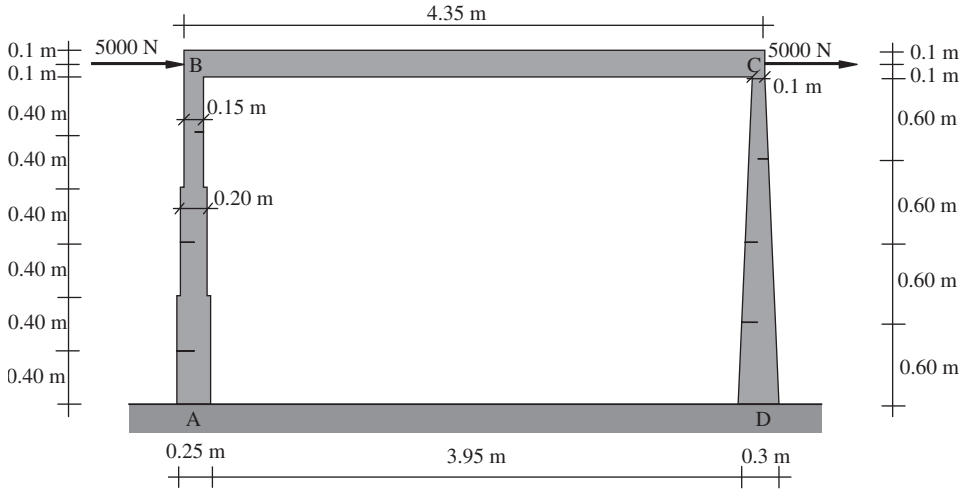


**Fig. 12.** Frame structure with multi-stepped column and column with linearly-varying height.

**Table 10**
Comparison of the representative values for second frame structure.

| Parameter | MCSBFE's | Standard FEs | COSMOS/M |
|---|---|---|---|
| No. elements | 3 | 104 | 15900 |
| No. nodes | 4 | 105 | 49681 |
| No. equations | 6 | 309 | 99218 |
| Displacement $u_B$ | 7.102 mm | 7.101 mm | 6.908 mm |
| Displacement $u_C$ | 7.102 mm | 7.101 mm | 6.908 mm |
| Force $H_A$ | 5012.686 N | 5012.370 N | 4867.894 N |
| Moment $M_A$ | 8488.781 Nm | 8488.250 Nm | 8104.225 Nm |
| Force $H_D$ | 4987.314 N | 4987.630 N | 5131.030 N |
| Moment $M_D$ | 9057.225 Nm | 9057.418 Nm | 9100.440 Nm |

Table 9 shows that the results from both line finite elements' models clearly converge. It is further evident that the disagreement of the results from 1D and 2D models is relatively small as maximum discrepancy (which appears with the bending-moment in the left support) is just slightly higher than 1.5%.

The non-cracked structure was also analysed implementing all three considered models and the agreement of the results (not presented) between 1D and 2D models was evidently even better.

*6.3.2. Second frame structure – multi-stepped column and column with linearly-varying height*

The second frame structure consisted of a multi-stepped column and a column with linearly-varying height (Fig. 12). This structure was obtained by replacing the multi-stepped right column from the previous frame structure by a column with linearly-varying height. Altogether six cracks were introduced to the structure and the adopted length for the beam was 4.225 m. In the second computational model, 100 beam finite elements of equal length and uniform heights were implemented to model the right column. The model's data, as well as some representative results are summarised in Table 10.

Similarly to the first frame structure it is evident from Table 10 that the results from both line finite elements' models clearly converge. However, it is further evident that the disagreement of the results from the 1D and 2D models is now slightly higher. Thus the maximum discrepancy for the displacement is 2.80%, whilst the maximum error for horizontal reaction (appearing at the left support) is 2.97%. Maximum discrepancy, again appearing at the bending moment in left support is 4.75%, which is now higher.

However, it should be mentioned that even when the non-cracked structure was analysed when implementing all three considered models, the agreement of the results (not presented)

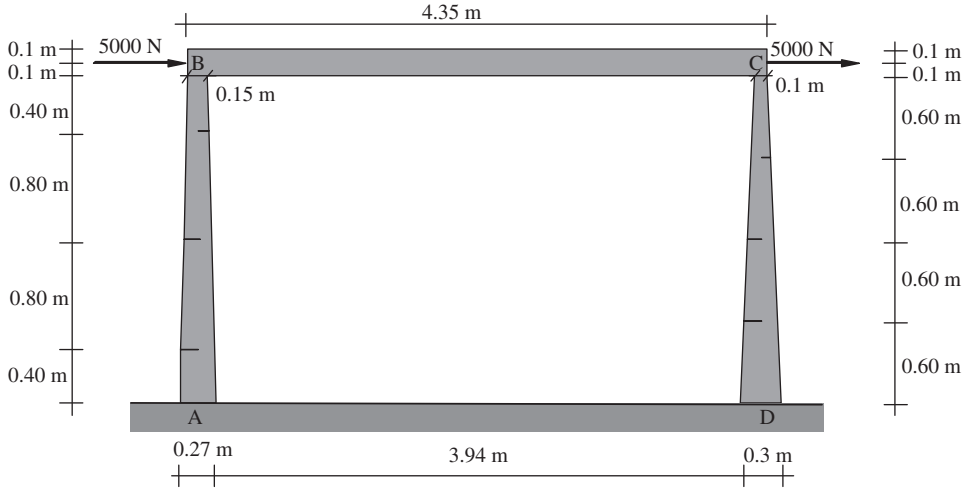


**Fig. 13.** Frame structure with two columns with linearly-varying height.

**Table 11**
Comparison of the representative values for third frame structure.

| Parameter | MCSBFE's | Standard FEs | COSMOS/M |
|---|---|---|---|
| No. elements | 3 | 201 | 14700 |
| No. nodes | 4 | 202 | 46046 |
| No. equations | 6 | 300 | 91988 |
| Displacement $u_B$ | 6.906 mm | 6.908 mm | 6.655 mm |
| Displacement $u_C$ | 6.907 mm | 6.909 mm | 6.657 mm |
| Force $H_A$ | 5117.479 N | 5115.666 N | 5008.542 N |
| Moment $M_A$ | 8625.486 Nm | 8618.330 Nm | 8313.368 Nm |
| Force $H_D$ | 4882.521 N | 4884.334 N | 4991.620 N |
| Moment $M_D$ | 8850.031 Nm | 8852.595 Nm | 8828.633 Nm |

amongst the 1D and 2D models was essentially no better. This indicates that the level of discrepancies is not influenced solely by cracks and their modellings, but also by the modelling details of the connection between the beam and columns with linearly-varying height.

*6.3.3. Third frame structure – two columns with linearly-varying height*

In the last frame structure the multi-stepped left column from the second frame structure was replaced by a column with linearly-varying height. The geometry of the newly-introduced column differed from the geometry of the right column (Fig. 13). Altogether six cracks were introduced to the structure and the adopted length for the beam was 4.225 m. In the second computational model each column was modeled by 100 beam finite elements of equal length and uniform heights. The model's data, as well as some representative results are summarized in Table 11.

Similarly to the both previously examined frame structures, it is evident from Table 11 that the results from both line finite elements' models again clearly converge. Further, the discrepancies of the results from the 1D and 2D models are somewhat comparable to the second frame structure. The maximum discrepancy for the displacement is now slightly higher (3.78%) whilst the discrepancies for horizontal reaction and bending moment are smaller. Thus, the maximum errors for horizontal reaction (appearing at right support) and the bending moment (in left support) are 2.19% and 3.75%, respectively.

The 1D and 2D models also produced similar levels of discrepancy for the non-cracked structure.

## 7. Conclusions

This paper studied multi-cracked slender-beams with the transverse cracks represented by means of internal hinges endowed by rotational springs. This simplified model was utilised for the derivation of a corresponding beam finite-element of a stepped cracked beam. The stiffness matrix, as well as the load vector due to a uniform continuous load were derived at by implementing the principle of virtual work. Despite the derivation's straightforwardness, all the obtained terms are written entirely in closed-symbolic forms that make the geometric as well as the damage parameters clearly observable. The provided expressions for geometric coefficients can even be numerically evaluated for any geometric variation of the beam's height, thus allowing the computational model to be expanded further than just stepped beams.

In the cases of multi-stepped beams with multiple cracks, the presented stiffness matrix, derived at by implementing the principle of virtual work, produces identical results to the solutions already proposed in the literature by other authors who have implemented different approaches. Therefore, in order to expand the topics, those beams with linearly-varying heights that appear more frequently, are also covered separately.

The derived at expressions introduced further new insights. The presented expressions namely condensed the complete damage parameters' impact into four coefficients only. Furthermore, the beam's geometric parameters are also covered by an additional four coefficients. These eight coefficients are clearly observable within the stiffness matrix and the load vector. The presented solutions clearly show that the geometric coefficients are dependable of the beam's height variation, whilst the damage coefficients are the same for arbitrary height's geometry. In addition, as just three damage coefficients impact on the stiffness matrix, this might even open-up new perspectives for the inverse identification of cracks.

The derivations implemented did not require any transverse displacements' shape-functions. Therefore, to complete the subject a computation of the considered model's accurate displacement functions was further accomplished where the expressions for stepped beams and beams with linearly-varying heights were derived at. Again, all the terms for both types of beams are presented in closed-forms that facilitate their implementation.

Three numerical examples follow the derivations. They demonstrated that elaborated solutions may be effectively implemented for structural analyses as the presented expressions produced excellent results that were confirmed independently by more thorough 2D models.

The derived at expressions thus offer – although short and compact – a reliable and efficient computational model. The presented finite element is consequently an optimum alternative for modelling any flexural cracks of beams and columns which is, for example, required by the European earthquake engineering design code EC8. The presented solutions are namely more efficient than both the alternative numerical solutions already available and allowed by the code. In comparison with detailed 2D and 3D models the solutions presented offer better computational efficiency without any essential lack of results' accuracy, whilst in contrast to the simple reduction of beam element's flexural rigidity they offer much better accuracy without any increase of the computational model.

The presented finite element can also be implemented within pushover analysis of a frame-type structure (in conjunction with concentrated plasticity's theory). Since the models allow for the local reduction of flexural rigidity this property can be implemented to model potential plastic hinges within an existing computational model with neither increase of the computational model nor additional remeshings.

Finally, as just three damage coefficients impact on the stiffness matrix, this might even open-up new perspectives for the inverse identification of multiple cracks.

## References

Bamnios, Y., Douka, E., Trochidis, A., 2002. Crack identification in beam structures using mechanical impedance. J. Sound Vib. 256 (2), 287–297.
Biondi, B., Caddemi, S., 2007. Euler–Bernoulli beams with multiple singularities in the flexural stiffness. Eur. J. Mech. A/Solids 26 (5), 789–809.
Boltežar, M., Štrancar, B., Kuhelj, A., 1998. Identification of transverse crack location in flexural vibrations of free-free beams. J. Sound Vib. 211 (5), 729–734.
Caddemi, S., Caliò, I., 2008. Exact solution of the multi-cracked Euler–Bernoulli column. Int. J. Solids Struct. 45 (16), 1332–1351.
Caddemi, S., Caliò, I., 2009. Exact closed-form solution for the vibration modes of the Euler–Bernoulli beam with multiple open cracks. J. Sound Vib. 327, 473–489.
Dado, M.H.F., Abuzeid, O., 2003. Coupled transverse and axial vibratory behaviour of cracked beam with end mass and rotary inertia. J. Sound Vib. 261, 675–696.
Dimarogonas, A.D., Papadopulus, C.A., 1983. Vibration of cracked shafts in bending. J. Sound Vib. 91 (4), 583–593.
Fernández-Sáez, J., Navarro, C., 2002. Fundamental frequency of cracked beams in bending vibrations: an analytical approach. J. Sound Vib. 256 (1), 17–31.
Gounaris, G., Dimarogonas, A.D., 1988. A finite element of a cracked prismatic beam for structural analysis. Comput. Struct. 28 (3), 301–313.
Hasan, W.M., 1995. Crack detection from the variation of the eigenfrequencies of a beam on elastic foundation. Eng. Fract. Mech. 52 (3), 409–421.
Khiem, N.T., Lien, T.V., 2001. A simplified method for natural frequency analysis of a multiple cracked beam. J. Sound Vib. 245, 737–751.

Kisa, M., Brandon, J., 2000. The effects of closure of cracks on the dynamics of a cracked cantilever beam. J. Sound Vib. 238 (1), 1–18.
Krawczuk, M., Ostachowicz, W.M., 1993. Influence of a crack on the dynamic stability of a column. J. Sound Vib. 167 (3), 541–555.
Krawczuk, M., Žak, A., Ostachowicz, W., 2000. Elastic beam finite element with a transverse elasto-plastic crack. Finite Elem. Anal. Des. 34, 61–73.
Li, Q.S., 2002. Free vibration analysis of non-uniform beams with an arbitrary number of cracks and concentrated masses. J. Sound Vib. 252, 509–525.
Lin, H.P., Chang, S.C., 2006. Forced responses of cracked cantilever beams subjected to a concentrated moving load. Int. J. Mech. Sci. 48, 1456–1463.
Maity, D., Saha, A., 2004. Damage assessment in structure from changes in static parameter using neural networks. Sadhana 29 (3), 315–327.
Okamura, H., Liu, H.W., Chorng-Shin, C., 1969. A cracked column under compression. Eng. Fract. Mech. 1, 547–564.
Ostachowicz, W.M., Krawczuk, M., 1990. Vibrational analysis of cracked beam. Comput. Struct. 36–22, 245–250.
Palmeri, A., Cicirello, A., 2011. Physically-based Dirac's delta functions in the static analysis of multi-cracked Euler–Bernoulli and Timoshenko beams. Int. J. Solids Struct. 48 (14–15), 2184–2195.
Rajab, M.D., Al-Sabeeh, A., 1991. Vibrational characteristics of cracked shafts. J. Sound Vib. 147 (3), 465–473.
Rizos, P.F., Aspraghtas, N., Dimarogonas, A.D., 1990. Identification of crack location and magnitude in a cantilever beam from the vibration modes. J. Sound Vib. 138, 381–388.
Sadowski, T., Marsavina, L., Peride, N., Craciun, E.-M., 2009. Cracks propagation and interaction in an orthotropic elastic material: analytical and numerical methods. Comput. Math. Sci. 46 (3), 687–693.
Shifrin, E.I., Ruotolo, R., 1999. Natural frequencies of a beam with an arbitrary number of cracks. J. Sound Vib. 222, 409–423.
Skrinar, M., 2007. On the application of a simple computational model for slender transversely cracked beams in buckling problems. Comput. Mater. Sci. 39 (1), 242–249.
Skrinar, M., 2009. Elastic beam finite element with an arbitrary number of transverse cracks. Finite Elem. Anal. Des. 45 (3), 181–189.
Skrinar, M., Pliberšek, T., 2004. New linear spring stiffness definition for displacement analysis of cracked beam elements. Proc. Appl. Math. Mech. 4, 654–655.
Skrinar, M., Pliberšek, T., 2012. On the derivation of symbolic form of stiffness matrix and load vector of a beam with an arbitrary number of transverse cracks. Comput. Mater. Sci. 52 (1), 253–260.
Skrinar, M., Umek, A., 1996. Plane beam finite element with crack. J. Gradbeni vestnik (in Slovenian) 1 (2), 2–7.
Sundermayer, J.N., Weaver, R.L., 1993. On crack identification and characterization in a beam by nonlinear vibration analysis. Theor. Appl. Mech., TAM, Report No. 743, UILU-ENG-93-6041.
Vestroni, F., 2009. Lecture Notes from the Course Dynamical Inverse Problems: Theory and Application, Udine.
Vestroni, F., Capecchi, D., 2000. Damage detection in beam structures based on frequency measurements. J. Eng. Mech. 126, 761–768.
Wang, J., Qiao, P., 2007. Vibration of beams with arbitrary discontinuities and boundary conditions. J. Sound Vib. 308, 12–27.
Xiang, J.W., Chen, X.F., Li, B., He, Y.M., He, Z.J., 2006. Identification of a crack in a beam based on the finite element method of a B-spline wavelet on the interval. J. Sound Vib. 296, 1046–1052.